Journal of Catalysis 280 (2011) 264–273

Contents lists available at ScienceDirect

Journal of Catalysis

journal homepage: www.elsevier.com/locate/jcat

Synthesis of methyl mercaptan from carbonyl sulfide over sulfide K_2MoO_4/SiO_2

Oliver Y. Gutiérrez [1], Christoph Kaufmann [1], Ana Hrabar, Yongzhong Zhu, Johannes A. Lercher *

Lehrstuhl für Technische Chemie 2, Technische Universität München, Lichtenbergstraße 4, D-85747 Garching, Germany

ARTICLE INFO

Article history:
Received 10 December 2010
Revised 23 February 2011
Accepted 26 March 2011
Available online 10 May 2011

Keywords:
Methyl mercaptan
Carbonyl sulfide
K-MoS_2
H_2S-containing synthesis gas

ABSTRACT

The synthesis of methyl mercaptan from COS and H_2 on K^+ promoted MoS_2 supported on silica is explored. The reaction proceeds via the disproportionation of COS to CO_2 and CS_2 and the consecutive hydrogenation of CS_2 to CH_3SH. In parallel to the disproportionation, COS also decomposes to CO and H_2S. The characterization of the catalyst by means of XRD, Raman spectroscopy, and adsorption of NO suggests that two active phases, i.e., relatively pure MoS_2 and K^+-decorated MoS_2, are present in the sulfided catalyst. The disproportionation of COS and the hydrogenation of CS_2 are favored on K^+-decorated MoS_2; the decomposition of COS to CO is the favored route on pure MoS_2. The reaction mechanisms for the decomposition of COS and the hydrogenation of CS_2 are discussed.

1. Introduction

Methyl mercaptan is an important chemical commodity widely used in the production of pesticides, pharmaceuticals, petrochemicals, and for material synthesis [1]. The main application of CH_3SH lies in the production of methionine, an amino acid used as an animal feed supplement [2]. With the rapid increase in the demand for methionine over the past 20 years, the demand for CH_3SH has been growing significantly [3]. Therefore, the synthesis of methyl mercaptan has been the subject of several studies and alternative routes for its production have been explored [4–6].

Industrially, methyl mercaptan is produced by thiolation of methanol. In this process, methanol and H_2S are reacted over alkali-promoted transition metal sulfides [1]. Considering that methanol is generated from synthesis gas, Olin et al. [7] proposed first to form CH_3SH directly from carbon oxides, hydrogen, and hydrogen sulfide. The catalysts for those reactions were based on alkali-promoted tungsten or molybdenum sulfides with transition metal oxides as additives [8]. The approach attracted significant interest, because it allowed avoiding the methanol synthesis step [9–14].

It is commonly accepted that the generation of CH_3SH from H_2S-containing syngas proceeds via the formation of carbonyl sulfide (COS) as the primary product and its subsequent hydrogenation to CH_3SH [15–17]. Preliminary experiments with COS as starting agent have indicated, however, that the direct hydrogenation of COS may not be a significant route.

The objective of this study was, therefore, to explore the synthesis of methyl mercaptan using COS, H_2, and H_2S as reactants. A two-step approach was adopted to achieve this goal, i.e., the selective production of COS followed by the synthesis of CH_3SH in a separate reactor. The formation of COS by reacting CO and H_2 with elemental liquid sulfur was reported elsewhere [18]. In this first step, CO conversion of 100% with high yield of COS at various reaction conditions was achieved. In the present work, we analyzed the catalytic synthesis of CH_3SH in the presence of H_2S over sulfided K_2MoO_4/SiO_2 by combining physicochemical characterization of the catalyst with detailed kinetic measurements. The thermodynamic equilibria of reactants and products were calculated to explore potential operating conditions.

2. Thermodynamic considerations

Calculations addressing the formation of CH_3SH from CO, H_2S, and H_2 have been reported by Barrault et al. [15]. Conversion of CO to methyl mercaptan is assumed to proceed via reactions (I) and (II).

$$CO + H_2S \rightleftharpoons COS + H_2 \quad (I)$$

$$COS + 3H_2 \rightleftharpoons CH_3SH + H_2O \quad (II)$$

The overall formation of methyl mercaptan from CO is thermodynamically allowed between 448 and 698 K and it is favored at high pressures and excess of H_2S and H_2. Here, only the thermodynamic calculations focusing on step (II) are reported. The conversion of COS as a function of temperature at various H_2/COS ratios and different total pressures is calculated using the HSC Chemistry 5.1 software. The results are compiled in Fig. 1-S of the supporting information. The lowest COS conversion is calculated for the stoichiometric ratio of H_2/COS = 3 (Fig. 1-Sa). Higher H_2/COS ratios increase the thermodynamically possible COS conversion. For

* Corresponding author. Fax: +49 89 28913544.
E-mail address: johannes.lercher@ch.tum.de (J.A. Lercher).
[1] The first two authors contributed equally to this work.

0021-9517/$ - see front matter © 2011 Published by Elsevier Inc.
doi:10.1016/j.jcat.2011.03.027

ratios higher than 4.5, a conversion of nearly 100% is possible up to 673 K. At higher temperatures, the maximum conversion of COS decreases, which is in line with the strongly exothermic nature of reaction (II), ($\Delta H^0 = -124$ kJ/mol).

Fig. 1-Sb shows the dependence of the COS conversion on the temperature at pressures ranging from 1 to 5 MPa. As reaction (II) proceeds, the number of total molecules decreases, and thus high pressures are favorable to maximize conversion. Considering the results of Barrault et al. [15] and the thermodynamic calculations described here, the synthesis of CH_3SH is studied at 3 MPa in the temperature range of 453–673 K with H_2/COS ratios from 2 to 7.

3. Experimental

3.1. Catalyst preparation and activation

A SiO_2 (AEROSIL® 90, Degussa) supported molybdenum sulfide catalyst, promoted with a twofold molar potassium excess over molybdenum, was used. The oxide precursor was synthesized by the incipient-wetness impregnation method using an aqueous solution of K_2MoO_4 (Sigma Aldrich, 98%). After impregnation, the catalyst precursor was dried at 353 K overnight and treated at 773 K in synthetic air for 12 h. The loading of K_2MoO_4 on SiO_2 was 28 wt.%. Prior to each activity test, 0.5 g of the catalyst was activated by sulfidation in 10 vol.% H_2S in H_2 at 3 MPa and 673 K for 12 h.

3.2. Kinetic measurements

Kinetic measurements were carried out by using two reactors in a serial configuration with a GC connected to the outlet of each reactor to monitor both steps as shown in Fig. 2-S of the supporting information. The first reactor was a semi-batch tank reactor (pre-reactor) used to obtain mixtures of COS and H_2S from the reaction of CO and H_2 (continuous reactants) with liquid sulfur (batch reactant). The configuration of the pre-reactor and the reactions taking place in it were described in detail elsewhere [18]. In this first step, the feed composition and reaction conditions were adjusted in order to achieve complete CO conversion and the H_2S/COS ratio required to perform the experiments in a subsequent plug-flow reactor with fixed catalyst bed (main reactor). The products from the pre-reactor were mixed with required concentrations of H_2 and N_2 prior to the second reaction step in the main reactor. Feed compositions reported in this work refer to the gas mixture introduced to the main reactor. The gas products were analyzed by gas chromatography using a Shimadzu GC 2014 equipped with a packed Haysep Q and a packed molecular sieve (13×) column.

3.2.1. Activity tests at varying H_2/COS and H_2S ratios

In the experiments at varying reactant ratios, the content of COS in the gas mixture was 8.6 vol.%, with N_2 being added to keep an overall reactant flow rate of 37 $cm^3\,min^{-1}$ (residence time of 0.68 s). The H_2/H_2S ratio was held constant at 4.5 to study the effect of the H_2/COS ratio, whereas a fixed H_2/COS ratio of 2.3 was chosen to study the effect of the H_2/H_2S ratio. GC measurements were taken in steps of 15 K from 453 to 673 K after steady state was achieved.

3.2.2. Activity tests at varying residence time

The effect of residence time on the reaction was studied at 523 and 598 K using constant ratios of H_2/COS = 2.3 and H_2/H_2S = 2.8. The mass of the catalyst was held constant (0.5 g), whereas the flow rates were varied in the range 6–60.5 $cm^3\,min^{-1}$ at 598 K and 12–40 $cm^3\,min^{-1}$ at 523 K. Residence time was defined as $v/V_{catalyst}$, where v is the volumetric flow rate and $V_{catalyst}$ is the total volume of the catalyst bed.

3.2.3. Activity tests in the absence of H_2

Experiments in the absence of H_2 were conducted to obtain a better understanding of the reactions in which COS is involved. At the end of a typical activity test in the presence of H_2, the reactor was flushed thoroughly with N_2 at 673 K to remove all reactants and products. After decreasing the temperature to 437 K, a total flow of 40 $cm^3\,min^{-1}$ of a gas mixture of 8.5 vol.% COS in N_2 was passed through the catalyst bed at 3 MPa. In the first experiment, the temperature was increased from 437 to 673 K in steps of 50 K, and the product was analyzed 5 min after reaching the desired temperature. In the second experiment, the temperature was increased from 437 to 523 K and kept constant for 5 h, and the products were analyzed every 50 min.

3.2.4. Catalytic test of bulk MoS_2 and sulfided K_2MoO_4

The sulfided form of bulk MoO_3 and K_2MoO_4 was tested in the reaction of COS with H_2. The reactor was loaded with 0.5 g of the oxide to perform the sulfidation in 10 vol.% H_2S in H_2 at 3 MPa and 673 K for 12 h. The overall reactant flow was 40 $cm^3 min^{-1}$ with a COS content of 8.6 vol.% and the ratios H_2/COS = 3 and H_2/H_2S = 5.3. The reaction temperature was increased from 448 to 598 K.

3.3. Elemental composition and textural properties

The elemental compositions of the oxide precursor and the used sulfide catalyst were determined by atomic absorption spectroscopy (AAS) using a UNICAM 939 spectrometer. The surface area and pore volume of the catalyst in the oxide and used sulfide forms were determined by nitrogen adsorption–desorption. The measurements were performed on a Porous Materials Incorporated automated BET sorptometer. Before adsorption, the samples were degassed in vacuum at 673 K for 2 h.

3.4. Raman spectroscopy

Raman spectra of the samples during the sulfidation–oxidation process were measured placing a sample of the catalyst in a suitable quartz tube reactor. The spectra of the oxide precursor were measured under N_2 at 290 K and under flow of 10 vol.% H_2S in H_2 at 290, 473, and 673 K. After sulfidation, the sample was cooled down to 290 K in N_2. New spectra were measured at 290 and 673 K after replacing N_2 by air. The Raman spectra were recorded on a Renishaw Raman Spectrometer Series 1000 Microscope with an Ar laser of 514 nm wavelength.

3.5. X-ray diffraction

The oxide precursor, the sulfide catalyst, and the catalyst used in the reaction were characterized by X-ray diffraction (XRD). Measurement of the sulfide catalyst was performed *ex situ*, after catalyst sulfidation for 12 h at 673 K and 3 MPa in 10 vol.% H_2S in H_2. A sample of the used catalyst was analyzed by XRD after cooling down the reactor to room temperature keeping the reactant mixture flow. The freshly sulfided catalyst and the sample of used catalyst were placed on a silicon single crystal with a (1 1 1) surface avoiding contact with air. Blank tests did not show any signals originating from the single crystal. A Philips X'Pert Pro System (Cu Kα1-radiation, 0.154056 nm) operating at 45 kV and 40 mA was used for recording XRD. Measurements were carried out using a step size of 0.017° (2θ) and 115 s as count time per step.

3.6. NO adsorption

Adsorption of NO on the catalyst was measured at room temperature by a pulse technique using a flow apparatus equipped with a mass spectrometer (QME 200, Pfeiffer Vacuum) as detector. For each experiment, a sample of 0.15 g was loaded in a quartz reactor and sulfided *in situ* (3 h at 673 K in 10 vol.% H_2S in H_2). In the first experiment, the sample was cooled down to room temperature in the H_2S/H_2 flow after sulfidation. NO pulses were periodically introduced after flushing the reactor with He. In the second experiment, the sample was cooled down to 523 K in the H_2S/H_2 flow after sulfidation and at constant temperature, the H_2S/H_2 flow was replaced by a COS/He mixture. After one hour, the sample was cooled down to room temperature in flowing COS/He. Subsequently, the sample was flushed with He and the NO pulses were applied at regular intervals. In both experiments, the total amount of adsorbed NO was calculated as the sum of the NO uptakes per pulse.

4. Results

4.1. Catalyst characterization

4.1.1. Composition and textural characteristics

The elemental composition in the oxide precursor determined by AAS analysis were 11.4 and 8.8 wt.% for molybdenum and potassium (corresponding to 5.85 and 11.08 mol%). The concentrations in the precursor mixture during the synthesis step were 11.3 and 9.2 wt.% for molybdenum and potassium, respectively. The oxide precursor has a specific surface area of 50 $m^2\ g^{-1}$ and pore volume of 0.06 $cm^3\ g^{-1}$.

The elemental composition of the used sulfide catalyst was 8.2, 6.2, and 9.5 wt.% for Mo, K, and S, respectively. Only traces of carbon were detected. The calculated S/Mo mol ratio was therefore 3.5, i.e., higher than the ratio expected for MoS_2 (S/Mo = 2), indicating that some sulfur was also associated with K^+ cations. The surface area and pore volume of the catalyst after reaction were 37 $m^2\ g^{-1}$ and 0.05 $cm^3\ g^{-1}$, respectively.

4.1.2. Raman spectroscopy

Fig. 1 shows the Raman spectra of the K_2MoO_4/SiO_2 catalyst recorded at different temperatures during the sulfidation–oxidation process. Spectrum (a) corresponds to the oxide K_2MoO_4/SiO_2 precursor in N_2 at 290 K with all bands being characteristic for K_2MoO_4 [19]. The widths of the bands at 849 and 711 cm^{-1}, however, suggest the presence of $K_2Mo_2O_7$ [20] and this conclusion is in agreement with findings by XRD (see below). New bands at 463 and 485 cm^{-1} after exposure to H_2S/H_2 at 290 K (Spectrum (b)) indicate the formation of K_2MoOS_3 [21]. Maintaining the H_2S/H_2 flow, the temperature was increased to 473 K for Spectrum (c). Bands appeared at 913 and 457 cm^{-1} are attributed to K_2MoS_4 [22]. After keeping the H_2/H_2S atmosphere for 4 h at 673 K, MoS_2 is detected as the main phase (450, 408, 382 cm^{-1}) as shown in Fig. 1d. After cooling the sample in N_2 flow to 290 K and applying synthetic air for 10 min, evidence of oxidation is not observed. Bands at 994, 816, 374, 336, 283, 237, and 219 cm^{-1} indicate the formation of MoO_3 after increasing the temperature to 673 K in synthetic air (Spectrum (e)) [23]. The bands at 964, 849 cm^{-1} and those in between correspond to the octamolybdate $K_4Mo_8O_{26}$ [19].

Detailed spectra of the sulfide catalyst are shown in Fig. 2. An example of the Raman spectra observed with the largest fraction of the sample is displayed in Spectrum (a). All bands are attributed to MoS_2 with those at 382, 408, and 450 cm^{-1} being the most intense [24]. The band at 382 cm^{-1} is assigned to the Mo-S stretching mode along the basal plane, while the one at 408 cm^{-1} corresponds to the S-Mo-S stretching mode along the C-axis. The band at 450 cm^{-1} is attributed to a second-order scattering [23]. At few spots of the sample (see Spectrum (b)), the bands at 1825, 1364, 911, 459, and ~200 cm^{-1} indicate the presence of a Resonance Raman Effect (RRE) typical for the MoS_4^{2-} ion [22,25]. Thus, we attribute these bands to K_2MoS_4 unevenly distributed in the solid.

The sequence of Raman spectra with the sulfidation in H_2S/H_2 atmosphere indicates that K_2MoS_4 is the first fully sulfided species formed, which is converted to MoS_2 in the next step. The Raman spectra do not allow deducing the location of all potassium cations. Some potassium cations remain in K_2MoS_4 that is not transformed to MoS_2 as indicated by the Raman spectra of the sulfide catalyst in Fig. 2b. The observation of MoO_3 and octamolybdates (K/Mo molar ratio of 0.5) after oxidation of the sulfide catalyst, however, suggests partial segregation of potassium from Mo-containing phases.

4.1.3. X-ray diffraction measurements

The X-ray diffractograms of the catalyst in the oxide and the sulfide form are shown in Fig. 3. The oxide precursor consists of a mixture of K_2MoO_4 (PDF number: 00-024-0880) and $K_2Mo_2O_7$ (PDF number: 00-036-0347), the latter phase is formed during thermal treatment in synthetic air. After sulfidation, most of the signals are characteristic of MoS_2 (PDF number: 00-024-0513).

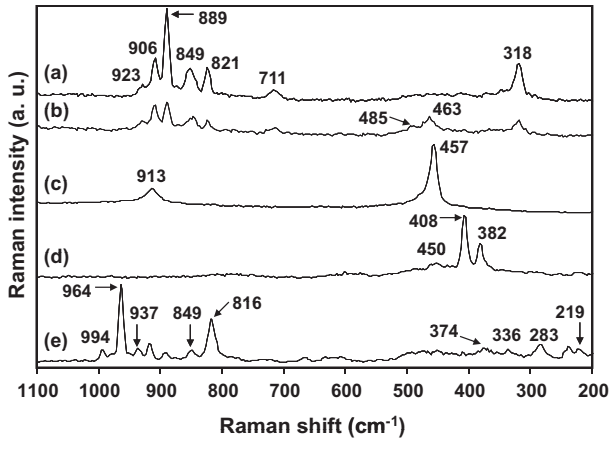

Fig. 1. Raman spectra of oxide K_2MoO_4/SiO_2 precursor in N_2 at room temperature (a), and after exposure to H_2S/H_2 at room temperature (b), to H_2S/H_2 at 473 K (c), to H_2S/H_2 at 673 K (d), and to synthetic air at 673 K (e).

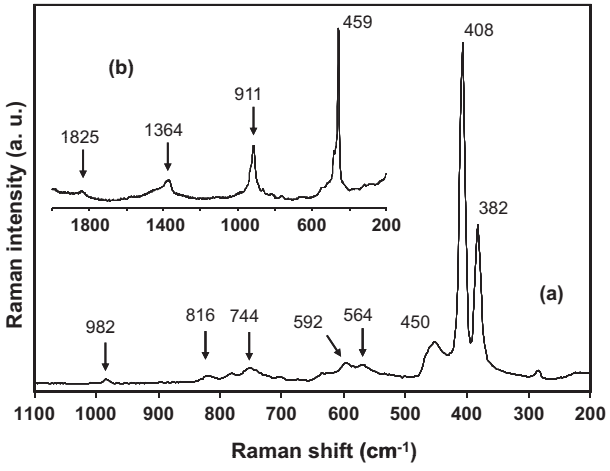

Fig. 2. Raman spectra of sulfide K_2MoO_4/SiO_2 catalyst observed typically (a) and in few spots of the sample (b).

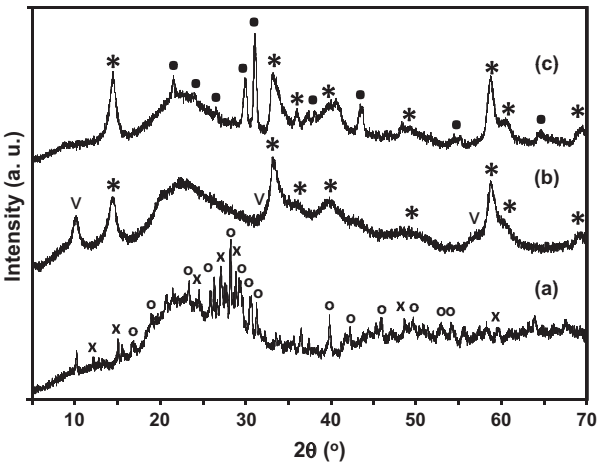

Fig. 3. XRD diffractograms of the oxide precursor (a), the sulfide K_2MoO_4/SiO_2 catalyst (b) and the catalyst after the reaction of COS and H_2 to CH_3SH (c). K_2MoO_4 (o), $K_2Mo_2O_7$ (x), MoS_2 (∗), K_xMoS_2 (v), and K_2SO_4 (●).

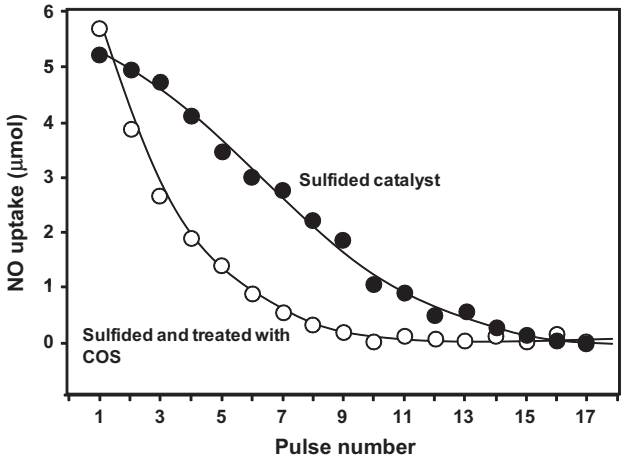

Fig. 4. NO uptake at room temperature over the freshly sulfided catalyst (●) and the sulfide catalyst exposed to COS/He flow at 523 K for 1 h (○).

The peak at 10.3° (2θ) cannot be assigned to a defined crystalline structure. We speculate that it corresponds to a K-intercalated MoS_2 (K_xMoS_2, $x < 1$). The position of that peak and the relative intensity of weak signals at 32.5 and 57.5° (2θ) are in accordance with the powder diffraction data reported for intercalated MoS_2 [26]. The formation of K_xMoS_2 (cationic potassium) takes place by the consecutive reactions (III) and (IV) [27].

$$K_2MoO_4 + 4H_2S \rightarrow K_2MoS_4 + 4H_2O \quad \text{(III)}$$

$$2K_2MoS_4 + 3H_2 \rightarrow 2K_xMoS_2 + (2-2x)K^0 + K_2S + 3H_2S \quad \text{(IV)}$$

The diffractogram of the used catalyst in Fig. 3 (line (c)) shows that the initial structure of the catalyst was not preserved under reaction conditions. The diffraction peaks attributed to K_xMoS_2 disappear, and new diffraction peaks corresponding to K_2SO_4 (PDF number: 00-003-0608) appear at 21.8, 23.9, 29.9, 31.1, and 43.6° (2θ). The formation of K_2SO_4 is consistent with the excess of sulfur found by elemental analysis in the used catalyst (S/Mo molar ratio of 3.5). The crystalline K_2SO_4 increases the density of the catalyst and blocks some pores leading to the decrease in surface area and pore volume per gram of material detected in the catalyst after activity tests.

According to reactions (III) and (IV), K_2MoS_4 was an intermediate in the sulfidation process, which was also indicated by the Raman spectra described above. A separate K_2S phase was not detected by XRD or Raman spectroscopy implying that it had to be highly dispersed and well-distributed in the catalyst. Under reaction conditions, however, it reacted readily and irreversibly with water leading finally to the agglomerated K_2SO_4 phase.

4.1.4. NO adsorption measurements

The concentration of NO adsorbed on coordinatively unsaturated metal cations at room temperature for the sulfided catalyst and the sulfided sample exposed to COS/He flow at 523 K are shown in Fig. 4. The corresponding peaks of the NO pulses are presented in Fig. 3-S in the supporting information. In both cases, the NO uptake is initially high, but decreases to zero as the maximum uptake capacity of the sample is reached. The NO uptake of the sample exposed to COS reaches steady state faster than the sample after sulfidation, i.e., the concentration of the accessible coordinatively unsaturated metal cations is much lower in the latter sample. The total NO concentration taken up for the as-sulfided sample is 229 μmol per gram of catalyst (molar ratio NO/Mo = 0.195), while the concentration of NO adsorbed on the COS pretreated sample is 113 μmol per gram of catalyst (molar ratio NO/Mo = 0.09).

4.2. Conversion of COS with varying H_2/COS ratio

Three different conditions were studied to evaluate the influence of the H_2/COS ratio, i.e., excess of hydrogen (H_2/COS = 7), near the stoichiometric ratio (H_2/COS = 4), and hydrogen deficient (H_2/COS = 2). The conversion of COS is presented in Table 1-S in the supporting information. The H_2/COS ratio had a strong effect on the conversion of COS. At 558 K, for example, the conversion of COS was 63% with H_2/COS = 2; it increased to 91% for H_2/COS = 4 and to 95% for H_2/COS = 7. The main products detected were CO_2, CO, and CH_3SH. CS_2 was also observed at low temperatures under H_2 deficient conditions. H_2O and traces of CH_4 were detected in the product stream above 560 K. Unfortunately, it was not possible to quantitatively determine the concentration of water. The yield of carbon oxides, CH_3SH, and CS_2 are shown in Fig. 5. CO was the main product at all temperatures with H_2/COS ratios of 7 and 4 and temperatures above 560 K at H_2/COS = 2. Fig. 5a shows that at a given temperature, the yield of CO_2 decreased with increasing H_2/COS ratio. At 560 K, for example, the yield of CO_2 decreased from 22% to 13% and 9.6%, when the H_2/COS ratio varied from 2 to 4 and 7, respectively. In contrast, the yield of CO increased with increasing H_2/COS ratio, for instance at 560 K, from 22 to 64 and 75% by increasing the H_2/COS ratio from 2 to 4 and finally to 7. Fig. 5b shows that CS_2 was observed only below 570 K at H_2/COS = 2 and below 510 K at H_2/COS = 4. CS_2 was not detected at higher H_2/COS ratios. The yield of CH_3SH reached its maximum at a H_2/COS ratio of 4 below 550 K. At higher temperatures, the yield of CH_3SH is favored by low H_2/COS ratio.

4.3. Conversion of COS with varying H_2/H_2S ratio

Three series of experiments were carried out at H_2/H_2S ratio of 3.1, 1.4, and 0.6, at a fixed H_2/COS ratio of 2.3. The conversion of COS was almost complete above 573 K and was not influenced by the H_2/H_2S ratio (see Table 2-S). The product yield is compiled in Fig. 6. The variation of the H_2/H_2S ratio did not affect the yield of carbon oxides significantly from 450 to 560 K. At higher temperatures, the increasing H_2/H_2S ratio led to a decrease in the yield of CO_2 and an increase in the yield of CO. Decreasing H_2/H_2S ratio decreased the yield of CS_2, but favored the yield of CH_3SH in the studied temperature range.

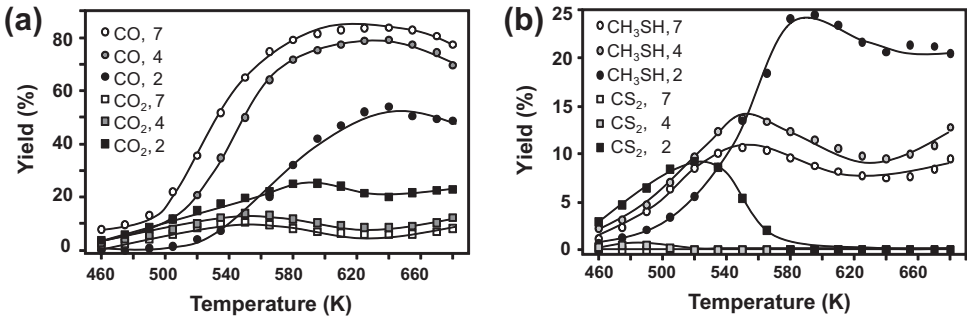

Fig. 5. Product yield on sulfide K_2MoO_4/SiO_2 at different H_2/COS ratios (white symbols 7, gray symbols 4, black symbols 2). CO (circles) and CO_2 (squares) (a); CH_3SH (circles) and CS_2 (squares) (b). 3 MPa, 37 cm^3 min^{-1} overall flow rate (residence time 0.68 s) and constant H_2/H_2S ratio of 4.5.

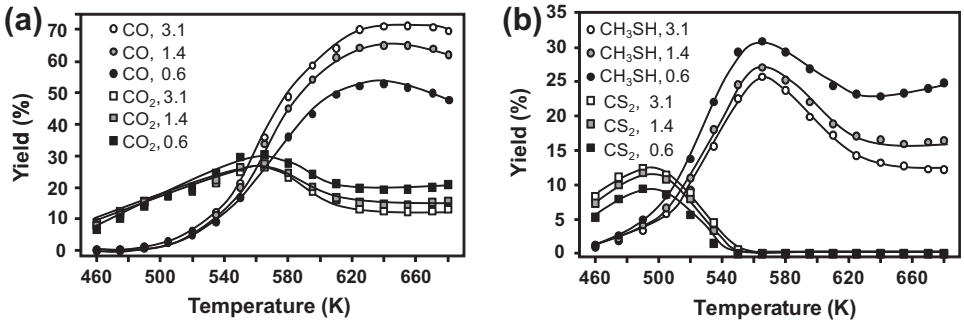

Fig. 6. Product yield on sulfide K_2MoO_4/SiO_2 at different H_2/H_2S ratios (white symbols 3.1, gray symbols 1.4, black symbols 0.6). CO (circles) and CO_2 (squares) (a); CH_3SH (circles) and CS_2 (squares) (b). 3 MPa, 37 cm^3 min^{-1} overall flow rate (residence time 0.68 s) and constant H_2/COS ratio of 2.3.

4.4. Conversion of COS with varying residence time

The effect of residence time was studied at 523 K and 598 K as shown in Fig. 7 in terms of selectivity (the corresponding yield at 523 K is shown in Fig. 10). At 523 K, the conversion of COS increased from 41% to 60% with increasing residence time, CS_2, CO, CO_2, and CH_3SH being the main products. The selectivity to carbon oxides was not affected to a significant extent by increasing the residence time; selectivity to CS_2, however, clearly decreased, whereas the selectivity to CH_3SH increased. At 598 K, the conversion of COS was above 96.5% in all experiments. Carbon oxides, methyl mercaptan, and a negligible amount of CH_4 were formed; CS_2 was not detected. At low residence time, CO was the main product; however, the selectivity to CO declined sharply at residence times higher than 0.72 s, while the selectivity to methyl mercaptan increased.

4.5. Catalytic tests in the absence of H_2

The product yields observed in the experiments performed in the absence of H_2 are shown in Fig. 8. In the first experiment (437–673 K), the conversion of COS increased from 23% to 29% (not shown here). At 437 K, CO_2 and CS_2 were the only products. CO was formed at 523 K, but declined afterward and only CO_2 and CS_2 were observed again. In the second experiment, the temperature was raised from 437 K to 523 K and then kept constant. At 437 K, only CO_2 and CS_2 were produced. At 523 K, CO was also observed, but declined afterward. This indicates that the formation of CO did not occur below 523 K and was residence time dependent at higher temperatures. In both experiments, H_2S was not detected, whereas CO_2 and CS_2 were observed in equimolar amounts pointing to disproportionation of COS.

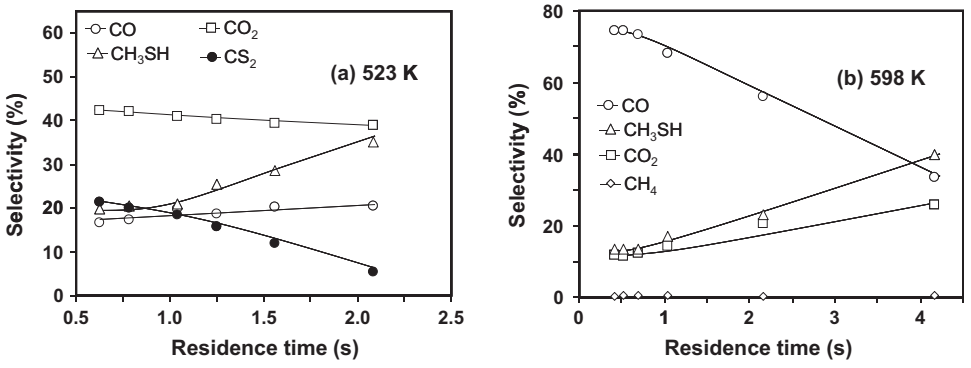

Fig. 7. Product selectivity as a function of residence time for the hydrogenation of COS over sulfide K_2MoO_4/SiO_2 at 3 MPa, 523 K (a) and 598 K (b). CO (○), CO_2 (□), CH_3SH (Δ) and CS_2 (●).

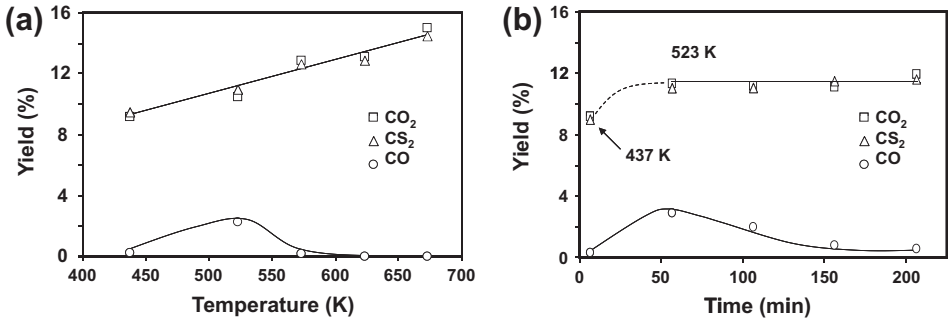

Fig. 8. Yield of CO (○), CO_2 (□), and CS_2 (Δ) obtained by passing a gas mixture of 8.5 vol.% COS in N_2 through the catalyst bed at 3 MPa and residence time 0.68 s. Yield as a function of increasing temperature (a) and time (isothermally at 523 K) (b). The first measurement in (b) was taken at 437 K.

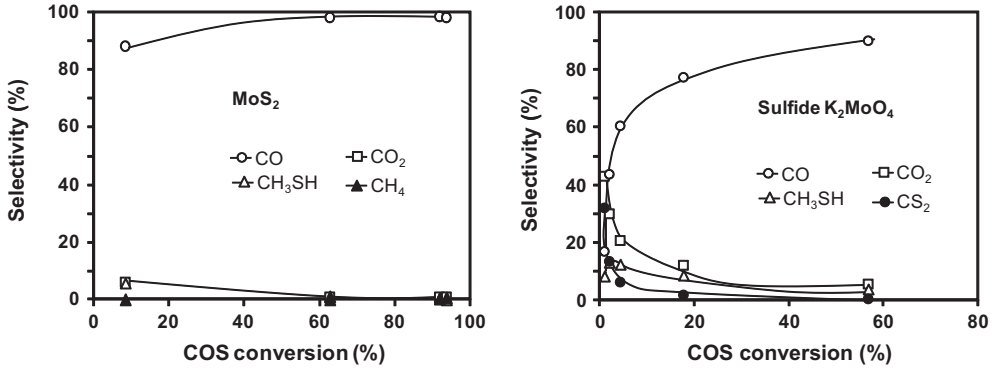

Fig. 9. Product selectivity as a function of COS conversion in the reaction of COS with H_2 on bulk MoS_2 and sulfided K_2MoO_4.

4.6. Catalytic test of bulk MoS_2 and sulfided K_2MoO_4

The selectivity obtained on bulk MoS_2 and sulfided K_2MoO_4 along with the conversion of COS is presented in Fig. 9. The corresponding yields are compiled in Tables 3-S and 4-S of the supporting information. With MoS_2, the preferred product was CO, whereas the selectivity to CO_2 and CH_3SH was very low. Only traces of CH_4 were observed. With sulfided K_2MoO_4, CO was the main product in most of the conversion range. Significant concentrations of the other products, however, were detected. The selectivity to CO_2 and CH_3SH was initially higher than that to CO, but decreased with COS conversion. CS_2 was detected at COS conversions below 20%.

5. Discussion

5.1. Evaluation of the reaction pathway

The conversion of COS as well as the CO yield increased rapidly at the temperatures from 498 to 538 K (see e.g., Table 1-S and Fig. 5) pointing to the direct hydrodecomposition of COS (V) in line with the thermodynamic equilibrium favoring CO in the reversible reaction $CO + H_2S \rightleftharpoons COS + H_2$ [28]. Thus, COS is concluded to rapidly decompose to CO and H_2S in accordance with the fact that the formation of COS by (I) is much faster than the subsequent reactions in the synthesis of CH_3SH from H_2S-containing syngas [15–17].

$$COS + H_2 \rightarrow CO + H_2S \quad (V)$$

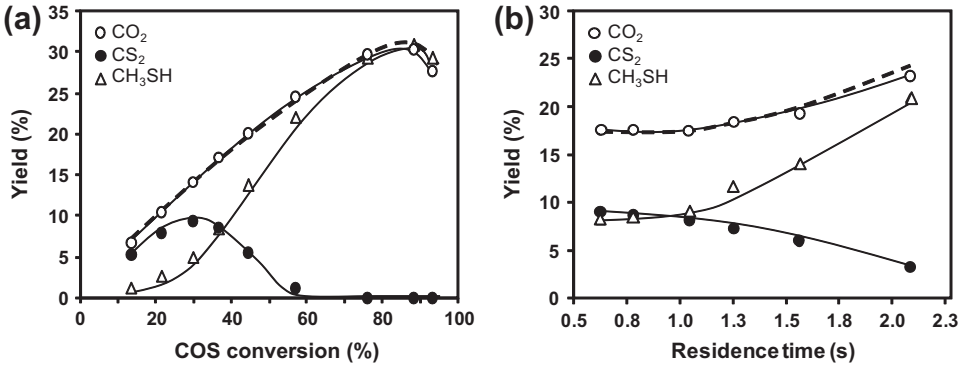

Fig. 10. Yield of CO_2 (○), CS_2 (●), and CH_3SH (Δ) over sulfide K_2MoO_4/SiO_2 as a function of COS conversion (a) and residence time at 523 K (b). The dashed line give the sum of the yield of CH_3SH and CS_2 (H_2/COS = 2.3, H_2/H_2S = 2.8).

CO_2 and CS_2 are formed by disproportionation of COS according to reaction (VI), as it was demonstrated by the experiments in the absence of H_2 (Fig. 8) in agreement with Ref. [16]. However, in the presence of H_2, the yield of CO_2 is always higher than the observed yield of CS_2 (see Fig. 6). This low CS_2/CO_2 ratio observed in the product stream is related to the reaction of CS_2 with hydrogen to form CH_3SH according to Eq. (VII). This is deduced from the fact that CS_2 is only detected at low temperatures and under H_2 deficient conditions and that the increase in the yield of CH_3SH occurs in parallel to the decrease in the CS_2 formation rate (see Figs. 5 and 6).

$$2COS \rightarrow CO_2 + CS_2 \quad (VI)$$

$$CS_2 + 3H_2 \rightarrow CH_3SH + H_2S \quad (VII)$$

Let us now discuss in depth the role of CS_2 in the reaction sequence. Fig. 10a shows the yield of CO_2, CS_2, and CH_3SH as well as the sum of the CS_2 and CH_3SH yield (dashed line) as a function of the conversion of COS ($H_2/H_2S = 0.6$). CO_2 and CS_2 are primary products. In contrast to CO_2, CS_2 is converted to CH_3SH at increasing COS conversion. The nearly equal concentration of CO_2 and of the sum of the concentrations of CS_2 and CH_3SH indicates that CS_2 is quantitatively converted to CH_3SH. While it should be noted that the points in Fig. 10a are constructed of data measured at different temperatures, the identical behavior is also observed, when the residence time is varied at 523 K (see Fig. 10b). This allows us to conclude that CH_3SH is solely produced by the hydrogenation of CS_2.

Methyl mercaptan is not formed by the direct hydrogenation of COS according to reaction (II), because it would imply that a parallel reaction would have to exist that forms CO_2 with a rate identical to the sum of the rates to CS_2 and CH_3SH and that all these reactions would have the same apparent energy of activation. These potential reactions to form CO_2 would be the hydrolysis of COS ($COS + H_2O \rightleftharpoons CO_2 + H_2S$) and the water gas shift reaction ($CO + H_2O \rightleftharpoons CO_2 + H_2$).

Fig. 10a also indicates that below conversion of 40% (500 K), the reaction (VII) is the rate determining step, because the CS_2 yield is higher than the yield of CH_3SH. At increasing temperature, the CH_3SH yield is higher than the CS_2 yield and at conversion of 60% (540 K) or above CS_2 is not detected. This implies that the rate of CS_2 hydrogenation exceeds that of the disproportionation of COS under these conditions, i.e., reaction (VI) becomes the rate determining step.

As it is shown that the disproportionation of COS to CO_2 and CS_2 is the first step of the overall reaction, CO_2 has to be formed at the same rate as CS_2 and CH_3SH together. This is the case below 573 K. Above 573 K, however, the rate of CO_2 formation is lower than the sum of the other two. Thus, CO_2 must be transformed at these temperatures. The possibilities for the decrease in the CO_2 yield are reactions (VIII) and (IX).

$$CO_2 + H_2 \rightleftharpoons CO + H_2O \quad (VIII)$$

$$CO_2 + H_2S \rightleftharpoons COS + H_2O \quad (IX)$$

To evaluate the relative rate of reactions (VIII) and (IX), the difference of the CH_3SH and the CO_2 yield in dependence of the H_2/H_2S ratio and the reaction temperature is presented in Fig. 11. It is noticed that the difference (CH_3SH yield and CO_2 yield) increased as the H_2/H_2S ratio decreased, i.e., the higher the concentration of H_2S the more CO_2 was consumed. Therefore, it is inferred that reaction (IX), in which CO_2 reacts with H_2S, dominates under the experimental conditions. Finally, the presence of traces of CH_4 at complete COS conversion (Fig. 7b) indicates the hydrogenation of methyl mercaptan to methane (reaction (X)).

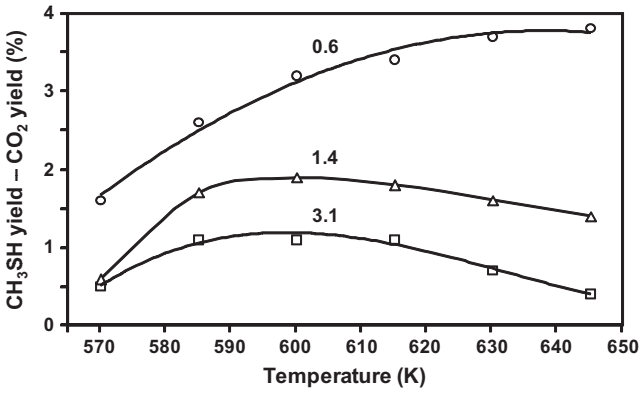

Fig. 11. Difference of the yield of CH_3SH and CO_2 (the CO_2 yield was subtracted from the CH_3SH yield) at $H_2/COS = 2.3$ and different H_2/H_2S ratios: 0.6 (o), 1.4 (Δ), and 3.1 (□).

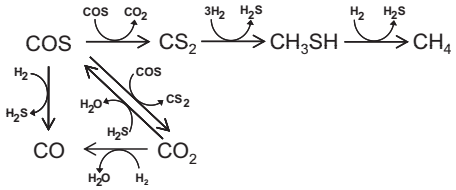

Fig. 12. Reaction pathway for the hydrogenation of COS over sulfide K_2MoO_4/SiO_2.

$$CH_3SH + H_2 \rightarrow CH_4 + H_2S \quad (X)$$

Thus, we conclude that the reaction pathway follows the routes depicted in Fig. 12. COS rapidly decomposes to CO and H_2S and in parallel disproportionates to CO_2 and CS_2. CS_2 is the species being hydrogenated to CH_3SH. At higher temperatures, CO_2 reacts with H_2S to form COS and H_2O, whereas the reaction to CO by the water gas shift reaction appears to be less significant. Methane is formed by hydrogenation of CH_3SH.

5.2. On the optimum conditions for the synthesis of CH_3SH from COS

The synthesis of methyl mercaptan proceeds through the COS disproportionation followed by the hydrogenation of CS_2. Clearly, the strategy to optimize the formation of methyl mercaptan either from H_2S-containing syngas or COS is to promote the COS disproportionation, CS_2 hydrogenation sequence, and to suppress the decomposition of COS. Increasing temperature and partial pressure of H_2 accelerate the production of CH_3SH. The rate of COS decomposition, however, increases faster than the rate of other reactions. Thus, the yield of methyl mercaptan is improved by increasing H_2/COS ratio only from 2 to 4 below 550 K, and the CH_3SH yield reaches its maximum values at 540–580 K decreasing at higher temperatures. The concentration of H_2S is beneficial for the CH_3SH yield by increasing the concentration of COS available for disproportionation via reaction (IX).

Thus, to optimize the yield of methyl mercaptan, it is necessary to apply concentrations of H_2 not higher than the stoichiometric concentration needed in the presence of H_2S and to limit the reaction temperature in a narrow range. For the system studied in this work, for instance, the optimum conditions are 580 K, $H_2/COS = 2$ and $H_2/H_2S = 0.6$. At this temperature, CS_2 is fully hydrogenated, whereas the yield of CO and CH_3SH is 36% and 31%, respectively.

The selectivity to CH_3SH can be further improved by modifying the catalyst formulation, e.g., using high surface area supports or adding a second promoter to the catalyst as shown in Ref. [29].

5.3. Active phases in the sulfide K_2MoO_4/SiO_2 catalyst

The catalytic activity observed is attributed to MoS_2, which is the main phase in the catalyst after sulfidation (XRD and Raman characterization) and is known to catalyze reactions involving heteroatoms [30–32]. The initial mixture of K_2MoO_4 and $K_2Mo_2O_7$ in the oxide precursor is transformed to MoS_2 by sulfiding as deduced from the *in situ* Raman spectra. In this process, the K^+ cations tend to segregate from Mo-containing species and only a minor fraction remains as K_2MoS_4 or is incorporated in the K_xMoS_2 phase (XRD of the sulfide catalyst). Because the K_xMoS_2 phase is not preserved during the reaction, we conclude that K^+ cations are not structurally associated with Mo-containing crystalline solids in the active material. However, K^+ cations decorate the MoS_2 surface as concluded from X-ray photoelectron spectroscopy (XPS) analysis of sulfide K_2MoO_4/SiO_2 catalyst (metal salt loadings close to 28 wt.%) [17]. For the studied catalyst, a fraction of K^+ adsorbs on MoS_2, while potassium species not associated with MoS_2 are speculated to form K_2SO_4 by reacting with oxidizing compounds (H_2O, CO_2) and H_2S under reaction conditions.

The segregation of the phases observed in the sulfidation–oxidation cycle (Fig. 1) suggests that not all the MoS_2 phase is decorated by K^+ probably due to the random distribution of K^+ on the surface. The MoO_3 observed in the reoxidized catalyst is speculated to be formed from K^+-free MoS_2, whereas $K_4Mo_8O_{26}$ forms from MoS_2 interacting with K^+ cations.

Thus, we conclude that two active phases, MoS_2 and K^+-decorated MoS_2, coexist in the sulfide K_2MoO_4/SiO_2 catalyst [33,34]. It is worth clarifying the difference between the K_xMoS_2 detected after sulfidation and the K^+-decorated MoS_2 phase. In the former structure, K^+ cations occupy defined positions, i.e., they intercalate between the MoS_2 slabs leading to additional reflections in the XRD pattern. In the K^+-decorated phase, the cations are distributed randomly on the MoS_2 surface, thus they do not modify the crystalline structure of the MoS_2 cluster. It is not possible to differentiate the pure MoS_2 phase and that decorated by K^+ by means of XRD.

The MoS_2 phase has coordinatively unsaturated sites (CUS) at the perimeter of the (1 0 1 0) plane, which act as active sites in hydrogenolysis and hydrogenation reactions [30–32]. The structure of the K^+-decorated MoS_2, i.e., the specific position of the K^+ cations with respect to the CUS remains unspecified. It has been proposed, however, that the presence of K^+ stabilizes oxygenated intermediates preventing C–O bond cleavage in the synthesis of alcohols and affects the electronic properties of the MoS_2 phase [35–37]. In the synthesis of CH_3SH from H_2S-containing syngas, the promoter effect of potassium on the selectivity has been related to the increasing concentration and the chemical environment of the Mo^{5+} that can be expected at the not completely coordinated Mo-edges interacting with oxidizing agents [17]. Thus, we conclude that the active sites in K^+-decorated MoS_2 are CUS. The presence of K^+ in the active phase, however, modifies the chemical and electronic environment of the active sites, i.e., the relative rate of hydrogenation and C–S bond cleavage.

Bulk MoS_2 and sulfide K_2MoO_4 were used in the reaction of COS with H_2 to clarify the role of MoS_2 and K^+-decorated MoS_2, which obviously has to form from the sulfided K_2MoO_4. Fig. 9 shows that the presence of K^+ increases drastically the selectivity to CO_2, CS_2, and CH_3SH and reduces the selectivity to CO. This is in line with the low conversion and poor CH_3SH yield obtained in the synthesis of methyl mercaptan from H_2S-containing syngas using unpromoted MoS_2 [14]. Thus, we conclude that the hydrodecomposition of COS takes place preferentially at MoS_2, whereas the disproportionation of COS and the consecutive hydrogenation of CS_2 is catalyzed faster on the K^+-decorated MoS_2 phase.

Note that the bulk sulfide K_2MoO_4 catalyst leads to very low conversion compared with the SiO_2-supported counterpart. This low activity is related to the low dispersion of the sulfides in that case. Also note in Fig. 9 that the difference in product selectivity between both bulk catalysts diminishes with increasing COS conversion. This is related to the fact that the points for high conversions have been measured above 540 K. At this high temperature, the decomposition to CO is favored over the other reactions and in consequence the promoter effect of potassium becomes less evident.

5.4. Active sites for the decomposition of COS

From the experiments performed in the absence of H_2, we deduce that the decomposition of COS to CO takes place at the CUS in MoS_2 as depicted in Fig. 13. COS first coordinates to the CUS in the MoS_2 structure. Then, the C-S cleavage results in CO desorption leaving the sulfur anion at the CUS. This is supported by the fact that the formation of CO stops in the absence of hydrogen (see Fig. 8) after some time on stream, implying that the reaction only occurs as long as accessible cations are available. Under the used reaction conditions, the CUS are regenerated by the reaction of hydrogen with the sulfur bridged Mo-edge of the active MoS_2 phase [38]. In contrast to the dissociation of COS, the disproportionation does not cease in the absence of H_2 indicating that it depends less or not at all on the presence of CUS in the MoS_2 phase.

Further evidence of the role of CUS in MoS_2 and K-promoted MoS_2 is obtained by NO adsorption. NO adsorbs on the CUS of promoted or unpromoted MoS_2, thus the concentration of NO adsorbed is correlated with the concentration of CUS in the catalyst [39,40]. In the pulse experiments, the NO uptake of the sample exposed to COS at 523 K was nearly 60% lower than the uptake of the fresh sulfided sample. This is in line with the mechanism in Fig. 13, because the concentration of CUS in the catalyst is drastically diminished after flowing COS in the absence of hydrogen. Furthermore, the disproportionation of COS occurs faster than the decomposition in the K^+-decorated MoS_2. Thus, the CUS in this phase are less susceptible to deactivation and remain able to adsorb NO.

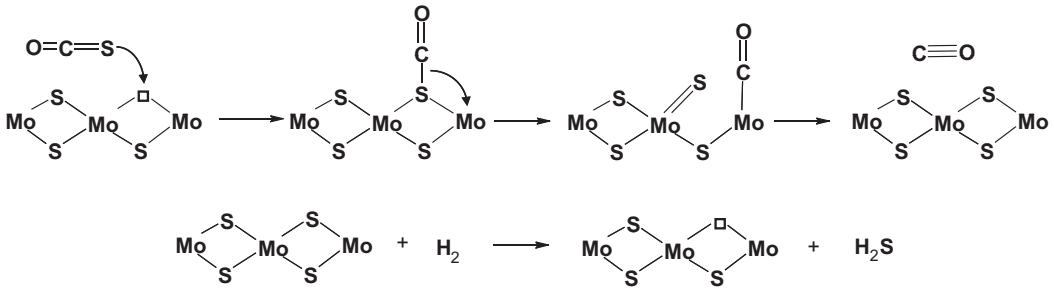

Fig. 13. Mechanism for the formation of CO from COS at the coordinatively unsaturated sites (CUS).

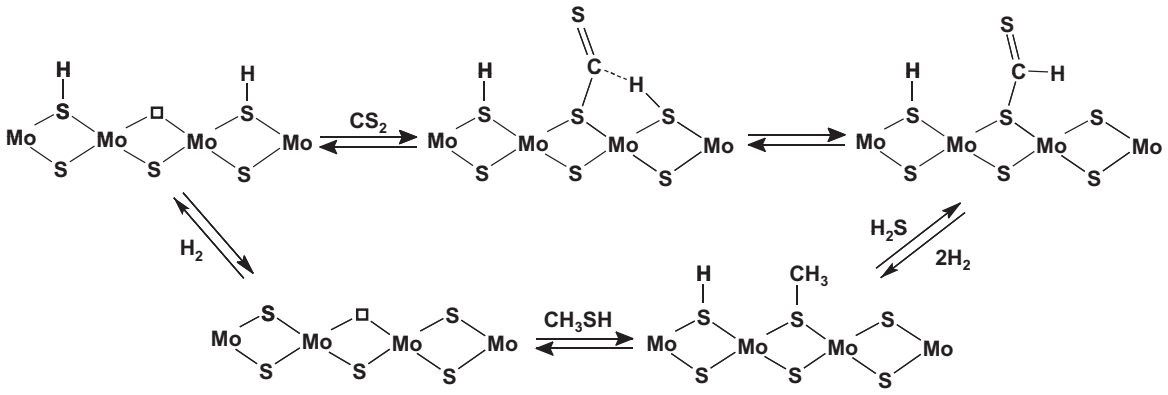

Fig. 14. Catalytic cycle for the hydrogenation of CS_2 to CH_3SH at the coordinatively unsaturated sites.

5.5. Active sites for the hydrogenation of CS_2

Two surface intermediates have been proposed for the direct hydrogenation of COS to methyl mercaptan, i.e., adsorbed thioformic acid (HSCHO) and adsorbed methanethiol (CH_3S) [16]. The former species has been postulated, but not observed, whereas the methanethiol fragment has been observed by vibrational spectroscopy on TiO_2, Al_2O_3, and MoS_2 [41–43]. Because the experiments reported here indicate that CS_2 is the species being hydrogenated, the intermediate formed cannot be related to thioformic acid, but rather to a dithioformic-based molecule. The postulated overall surface process that leads to the formation of methyl mercaptan is illustrated in Fig. 14. CS_2 coordinates to a CUS in the first step. Then, a nearby hydrogen atom reacts with the adsorbed CS_2 to form a HSCS species. It has been confirmed by spectroscopic techniques and *ab initio* calculations that the reaction between hydrogen atoms and CS_2 to form the HSCS species is spontaneous and has low activation energy [44]. The rearrangement and interaction of the HSCS fragment with hydrogen leads to the release of a H_2S molecule and one adsorbed methanethiol. Then, the combination of the adsorbed methanethiol with hydrogen in the surface releases the methanethiol, whereas the hydrogen atoms adjacent to the CUS are generated by dissociative adsorption of H_2.

At present, the exact mechanism of the rearrangement of the HSCS species to adsorbed methanethiol can only be derived from *ab initio* DFT calculations. The combination of a second hydrogen atom with the HSCS species leads to the formation of a dithioformic acid fragment (HCSSH) [45,46]. The decomposition of dithioformic acid can take place by dehydrogensulfidation yielding H_2S and C=S or by dehydrogenation to CS_2 and H_2 [46,45]. The former mechanism is favored over the dehydrogenation which is well in line with the necessary H_2S release from the adsorbed dithioformic acid to form the methanethiol fragment (see Fig. 14). Interestingly, the two pathways for the HCSSH decomposition can be assisted by H_2 or H_2S and can comprise the formation of a dithiohydroxy carbene (HSCSH). This species, adsorbed in a CUS, could form the methanethiol fragment after H_2S release and hydrogenation.

Although the adsorbed species could interact directly with molecular hydrogen from the gas phase, the hydrogen provided by the surface SH groups seems to play a key role in the hydrogen addition steps in the mechanism of Fig. 14. Chen et al. [17,29] have reported the XPS characterization of sulfided K_2MoO_4/SiO_2 catalysts and the synthesis of methyl mercaptan from syngas. In that report the yield of CH_3SH was related to the concentration of low valence Mo and S species, i.e., $(S–S)^{2-}$ and $Mo^{4+}–S^{2-}$. These species form SH groups by heterolytic or homolytic dissociation of hydrogen [47,48]. Furthermore, the SH groups formed by the interaction of the sulfide surface with H_2 or H_2S under reaction conditions are claimed to provide the hydrogen in hydrotreatment applications [49–51]. As the active sites in MoS_2 and K^+-MoS_2 are fundamentally the same (CUS), the hydrogenation of CS_2 can take place on both phases. The presence of K^+, however, could promote the hydrogenation of CS_2, because it could increase the concentration of SH groups in the surface via adsorption of H_2S ($K^+ + H_2S + S^{2-} \rightleftharpoons K–SH + SH$).

6. Conclusions

The synthesis of CH_3SH over sulfide K_2MoO_4/SiO_2 is explored using COS, H_2, and H_2S as educts. COS decomposes rapidly to CO and H_2S. In parallel, COS disproportionates to CO_2 and CS_2. CS_2 is the reaction intermediate that is hydrogenated to CH_3SH. CO_2 and CH_3SH are consumed at high temperatures. CO_2 reacts with H_2S to COS and H_2O, while the reverse water gas shift reaction can take place to a lower extent. CH_3SH is further hydrogenated to CH_4.

During the sulfidation reaction, the main phases present in the catalyst are MoS_2, K^+-promoted MoS_2, and K_2SO_4. The MoS_2 phase catalyzes the decomposition of COS to CO, whereas the disproportionation of COS and subsequent hydrogenation of CS_2 is faster on the K^+-decorated MoS_2 phase. The active sites in both phases for the decomposition of COS and hydrogenation of CS_2 are CUS. The role of the K^+ cations in the K^+-decorated MoS_2 phase is to accelerate the rates of the disproportionation of COS and of the hydrogenation of CS_2.

Acknowledgment

The authors gratefully acknowledge Evonik Degussa GmbH (Germany) for fruitful discussion and financial support.

Appendix A. Supplementary material

Supplementary data associated with this article can be found, in the online version, at doi:10.1016/j.jcat.2011.03.027.

References

[1] J. Sauer, W. Boeck, L. von Hippel, W. Burkhardt, S. Rautenberg, D. Arntz, W. Hofen, US patent 5 852 219, 1998.
[2] Y. Yang, S. Dai, Y. Yuan, R. Lin, D. Tang, H. Zhang, Appl. Catal. A 192 (2000) 175.
[3] W. Leuchtenberger, K. Huthmacher, K. Drauz, Appl. Microbiol. Biotechnol. 69 (2005) 1.
[4] B. Buchholz, US patent 4 410 731, 1983.
[5] M. Boulinguiez, C. Forquy, J. Barrault, US patent 4 665 242, 1987.
[6] Y. Yang, Q. Wang, R. Lin, H. Zhang, Y. Yuan, W. Fang, Z. Quanxing, D. Shenjun, X. Yan, A. Chen; J-O. Barth, C. Weckbecker, K. Huthmacher, H. Redlingshoefer; S. Ackermann, US patent 7 569 731, 2009.

[7] J. Olin, B. Buchholz, B. Loev, R. Goshorn, US patent 3 070 632, 1960.
[8] P. Haines, US patent 4 449 006, 1984.
[9] D. Kubicek, US patent 4 120 944, 1978.
[10] I. Wachs, GB patent 2 344 343, 1998.
[11] C. Ratcliffe, P. Tromp, US patent 4 668 825, 1987.
[12] B. Zhang, S. Taylor, G. Hutchings, New J. Chem. 28 (2004) 471.
[13] Y. Yang, Y. Yuan, S. Dai, B. Wang, H. Zhang, Catal. Lett. 54 (1998) 65.
[14] Y. Yang, H. Yang, Q. Wang, L. Yu, C. Wang, S. Dai, Y. Yuan, Catal. Lett. 74 (2001) 221.
[15] J. Barrault, M. Boulinguiez, C. Forquy, R. Maurel, Appl. Catal. 33 (1987) 309.
[16] G. Mul, I. Wachs, A. Hirschon, Catal. Today 78 (2003) 327.
[17] A. Chen, Q. Wang, Q. Li, Y. Hao, W. Fang, J. Mol. Catal. A 283 (2008) 69.
[18] C. Kaufmann, O. Gutiérrez, Y. Zhu, J. Lercher, Res. Chem. Int. 36 (2010) 211.
[19] N. Verbruggen, G. Mest, L. von Hippel, B. Lengeler, H. Knözinger, Langmuir 10 (1994) 3063.
[20] V. Kettmann, P. Balgavy, L. Sokol, J. Catal. 112 (1988) 93.
[21] A. von Müller, H. Schulze, W. Sievert, N. Weinstock, Z. Anorg. Allg. Chem. 403 (1974) 310.
[22] A. Ranade, M. Stockburger, Chem. Phys. Lett. 22 (1973) 257.
[23] G. Schrader, C. Cheng, J. Catal. 80 (1983) 369.
[24] A. Stacy, D. Hodul, J. Phys. Chem. Solids 46 (1985) 405.
[25] W. Kiefer, H. Bernstein, Chem. Phys. Lett. 8 (1971) 381.
[26] R. Somoano, V. Hadek, A. Rembaum, J. Chem. Phys. 58 (1973) 697.
[27] F. Wypych, C. Solenthaler, R. Prins, Th. Weber, J. Solid State Chem. 144 (1999) 430.
[28] F. Farhad, I. Safarik, O. Strausz, M. Torres, E. Yildirim, Ind. Eng. Chem. Res. 35 (1996) 3854.
[29] A. Chen, Q. Wang, Y. Hao, W. Fang, Y. Yang, Catal. Lett. 118 (2007) 295.
[30] A. Startsev, Catal. Rev. – Sci. Eng. 37 (1995) 353.
[31] R. Chianelli, M. Siadati, M. De la Rosa, G. Berhault, J. Wilcoxon, R. Bearden Jr., B. Abrams, Catal. Rev. 48 (2006) 1.
[32] M. Breysse, E. Furimsky, S. Kasztelan, M. Lacroix, G. Perot, Catal. Rev. – Sci. Eng. 44 (2002) 651.
[33] M. Jiang, G. Bian, Y. Fu, J. Catal. 146 (1994) 144.
[34] J. Lee, S. Kim, K. Lee, I. Nam, J. Chung, Y. Kim, H. Woo, Appl. Catal. A 110 (1994) 11.
[35] A. Anderson, J. Yu, J. Catal. 119 (1989) 135.
[36] Y. Li, R. Wang, L. Chang, Catal. Today 51 (1999) 25.
[37] K. Park, J. Kong, Top. Catal. 18 (2002) 175.
[38] F. Dumeignil, J. Paul, E. Veilly, E. Qian, A. Ishihara, E. Payen, T. Kabe, App. Catal. A 289 (2005).
[39] Y. Okamoto, M. Kawano, T. Kubota, Chem. Commun. 9 (2003) 1086.
[40] N. Topsøe, H. Topsøe, J. Catal. 84 (1986) 386.
[41] D. Beck, J. White, C. Ratcliffe, J. Phys. Chem. 90 (1986) 3132.
[42] O. Saur, T. Chevreau, J. Lamotte, J. Travert, J. Lavalley, J. Chem. Soc. Faraday Trans. 1 77 (1981) 427.
[43] A. Tsyganenko, F. Can, A. Travert, F. Maugé, Appl. Catal. A 268 (2004) 189.
[44] R. Bohn, G. Brabson, A. Lester, J. Phys. Chem. 96 (1992) 1582.
[45] X. Xie, Y. Tao, H. Cao, W. Duang, Chem. Phys. 213 (1996) 133.
[46] M. Nguyen, T. Nguyen, H. Le, J. Phys. Chem. A 103 (1999) 5758.
[47] J. Spirko, M. Neiman, A. Oelker, K. Klier, Surf. Sci. 572 (2004) 191.
[48] A. Startsev, I. Zakharov, V. Parmon, J. Mol. Catal. A 192 (2003) 113.
[49] J. Lipsch, G. Shuit, J. Catal. 15 (1969) 179.
[50] H. Kwart, G. Shuit, B. Gates, J. Catal. 61 (1980) 128.
[51] F. Bataille, J. Lemberton, P. Michaud, G. Pérot, M. Vrinat, M. Lemaire, E. Schultz, M. Breysse, S. Kasztelan, J. Catal. 191 (2000) 409.